SPIF accuracy improvement by FEM analysis of multi-step tool trajectories with experimental validation

Cristian Cappellini[1,a] *, Claudio Giardini[1,b] and Sara Bocchi[1,c]

[1]University of Bergamo, Department of Management, Information and Production Engineering, Via Pasubio 7/b, 24044 Dalmine (BG), Italy

[a]cristian.cappellini@unibg.it, [b]claudio.giardini@unibg.it, [c]sara.bocchi@unibg.it

Keywords: Incremental Sheet Forming, Accuracy, Finite Element Method (FEM)

Abstract. This study focuses on the application of Single Point Incremental Forming (SPIF) in modern manufacturing, particularly in batch production where flexibility and cost-efficiency are crucial. SPIF enables forming various shapes with reduced tool-workpiece contact and minimal forming forces. A critical factor affecting product quality is the tool trajectory, which influences material springback and accuracy, leading to issues like geometric deviations and defects such as the pillow effect. To address these challenges, the research proposes Finite Element Method (FEM) simulations to analyze alternative SPIF multi-step tool paths. Focusing on frustum cones made of AA1050-H24 aluminum alloy, the study compares simulation results with experimental data, highlighting a roughing-finishing approach that improves geometric accuracy and reduces defects, making it viable for industrial use.

Introduction

Following the Industry 4.0 paradigms, enterprises shifted from mass to batch production, where higher flexibility and lower asset costs are mandatory [1]. Considering this, the capability of working several materials in die-less condition with a generic tool, individuates Single Point Incremental Forming (SPIF) as an appropriated forming alternative [2]. Despite dedicated machines has been developed to accomplish SPIF, its application on generic 3-axis CNC and robot-based machines, further enhancing process flexibility, was demonstrated [2]. SPIF is performed by a sequential movement of the forming tool on a blank, by following different paths at increasing penetration depths, as a function of desired shape and axial deepness. This results in a reduced tool-workpiece contact area, with low forming forces and increased material formability [3]. Numerous studies recognized tool trajectory as one of the most influencing parameters on the quality of the final product [4-6]. Each selected tool trajectory, in fact, causes a determined material displacement, influencing material work-hardening and related springback [7]. This leads to reduced accuracy, defined as the deviation of the part geometry from the nominal one. In this sense, multi-step tool path methodology demonstrated to beneficially affect material formability [8], while issues regarding accuracy remain still open. Despite in the production of cylindrical parts, multi-stage SPIF allows to obtain high precision vertical walls, it introduces rigid body motion (RBM) phenomena, resulting in stepped features that compromise the bottom quality [9]. Multi-pass associated stepped features were also observed in [10,11], hence, with the aim of reducing RBM, a multidirectional tool path was proposed in [12], but with poor results. Similarly, pillow defect, a bulging effect on the bottom, was detected in the manufacturing of conical squared cup exploiting sequential tool steps [13], revealing the achievement of a flat bottom part as one of the most difficult task. In order to reduce expensive and time-consuming experimental tests, Finite Element Method (FEM) simulation method was widely employed for analyzing SPIF process. In [14] simulations applying different element types were developed for predicting SPIF forces, with good results of both solid and shell elements. A reliable SPIF loads forecast was achieved in [15] as well, where a sub-modeling technique was implemented to refine the blank-tool contact area.

Materials Research Proceedings 52 (2025) 67-75 https://doi.org/10.21741/9781644903551-9

Alternative multi-stage tool paths were studied by FEM in [16] improving thickness distribution in vase shaped parts. For validating a deflection model, FEM was used in [17] allowing to estimate springback on walls and in the contact zone. FEM models studying the effect of process parameters in vacuum assisted SPIF, obtaining a close comparison with experimental results, were developed [18]. A good match was also achieved in [19] where the effects of varying dimensions shaped tools on the amount of pillow defect were evaluated.

Considering this, the present work proposes a FEM investigation of the influence of alternative SPIF multi-step tool trajectories on the geometric accuracy of frustum cones made of AA1050-H24 aluminum alloy. Aimed to minimize wall deviation and pillow effect, these strategies were analyzed by experimentally validated FEM simulations. The comparisons of nominal and simulated geometries, the resulting thickness distributions, and the estimated forming loads, allowed to individuate a roughing-finishing approach giving encouraging quality outcomes even exploitable under an industrial point of view.

The analyzed multi-step tool trajectories

Five different tool paths (Fig. 1), one concerning a single-step and four regarding multi-step strategies, developed for producing frustum cone geometry (Fig. 2a), were investigated by FEM simulations. Fig. 1 reports the values of the employed geometrical parameters as well.

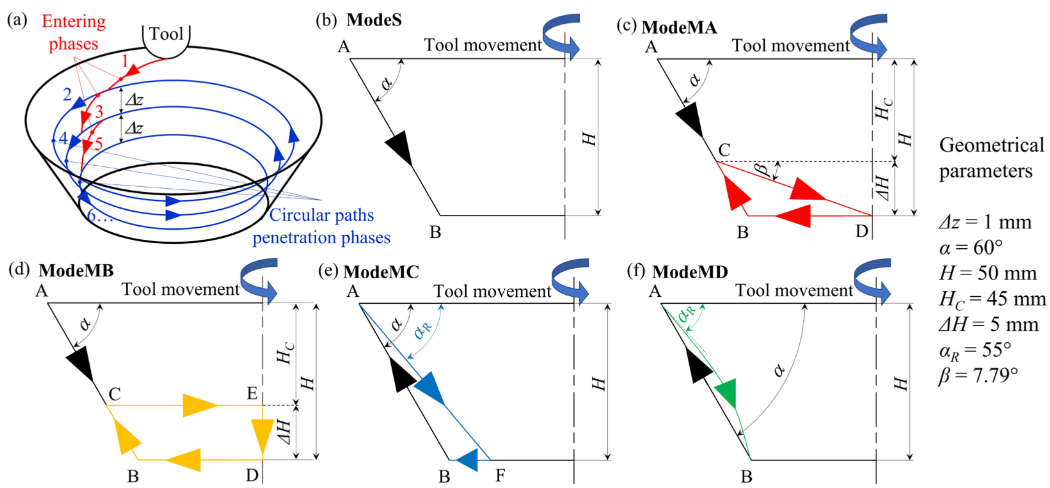

Fig. 1 Schematic of the analyzed tool path strategies with geometrical parameters' values.

Fig. 1b reports the employed single-step path ModeS (helical tool path described by Fig. 1a). In ModeS the tool follows a circular path at a determined axial depth. After this, the tool moves downward of a quantity Δz (step down) to cover a new circular path. This procedure is repeated until reaching the bottom of the frustum cone (depth H) with a circular path diameter in accordance with the desired wall angle α. ModeMA (Fig. 1c) concerns a multi-step strategy where the initial step is analogous to ModeS until a cone depth of H_C. Form this position, the tool moves following a lower wall angle β up to the bottom depth H at constant reduced Δz values according to the $\tan(\beta)/\tan(\alpha)$ ratio. Then, the tool describes a spiral path to enlarge the bottom at the desired radial position (point B). Subsequently, the tool displacement follows the α angle by the initial constant value of Δz up to depth H_C. ModeMB (Fig. 1d) represents a tiny modification of multi-step ModeMA in which, at depth H_C, the tool shifts to the cone center (point E) and then axially penetrates to bottom depth H. The movement of the tool over D-B and B-C lines is the same performed in ModeMA. As suggested in [16], the remaining penetration depth ΔH was chosen equal to the 10 % of the height H, for minimizing RBM, resulting in a β angle connecting C with the bottom center D. ModeMC (Fig. 1e) consist of a multi-step strategy where a first roughing step, concerning a wall angle α_R narrower than α, is achieved following ModeS to the bottom depth

H (point F). Afterward, the bottom surface is enlarged to desired point B by a spiral tool movement where the finishing step, realized for achieving the desired wall angle α (B-A) at constant Δz, starts. ModeMD (Fig. 1f) denotes again a roughing-and-finishing multi-step strategy where, the former step realizes an increasing wall angle from the top (α_R in point A) to the desired angle α at the bottom (point B), while the latter is performed at constant α and Δz from bottom to top. The choice of forming the bottom was performed trying to reduce the amount of pillow defect. The α_R value in ModeMC was selected to achieve a reduced length of F-B on the bottom to contain sheet stretching and thinning.

FEM simulations setup and experimental validation

The FEM simulation setup was calibrated and then validated by comparing the experimental results (final geometry, forming forces, and material thickness) with the simulated ones, in the production of frustum cone (Fig. 2a). The calibration referred to ModeS strategy, while the final validation to ModeMD. The experiments were performed on a MC-60 Evolution 3-axis CNC machine having provide with a 18i-M GE Fanuc numerical control. The initial blank was a 1 mm in thickness AA1050-H24 aluminum sheet (Table 1), having a squared shape with a cantilevered edge length of 150 mm. Along the SPIF process, the blank was supported by a specifically designed equipment, allowing to acquire the forming forces, shown in Fig. 2b. For measuring the three components of the force, a Kistler 9257BA load cell, having a range of ±5 kN for *X*-*Y* components and from -5 kN to +10 kN for the *Z* one, was exploited. It was then connected to a control unit (Kistler Type 5223A) sending the forces' signals to a Hottinger Brüel & Kjær® Catman Data Acquisition Software. This latter was used for realizing a dedicated interface able to acquire the signals at a frequency of 200 Hz. The applied tool was a hemispherical one with a radius r = 10 mm, made of AISI 1045 steel. During the SPIF tests it moves with both constant feed rate of 600 mm/s and Δz of 1 mm. It was free to rotate and no spindle speed was assigned to it. The tests were performed in lubricated conditions using grease. In conformity to the cone geometry and tool dimensions, NC programs were prepared exploiting the Autodesk Fusion 360® CAD/CAM interface. The geometries of the produced frustum cones were acquired by the Hexagon® RA-8525-7 scanning system, consisting of a scanner (model AS1) coupled to a 7-axis arm. The achieved point cloud geometry was then fixed and exported as a STL file utilizing PolyWorks® software. Once the frustum cone geometry was attained, it was trimmed on the diametral section for measuring the thickness distribution.

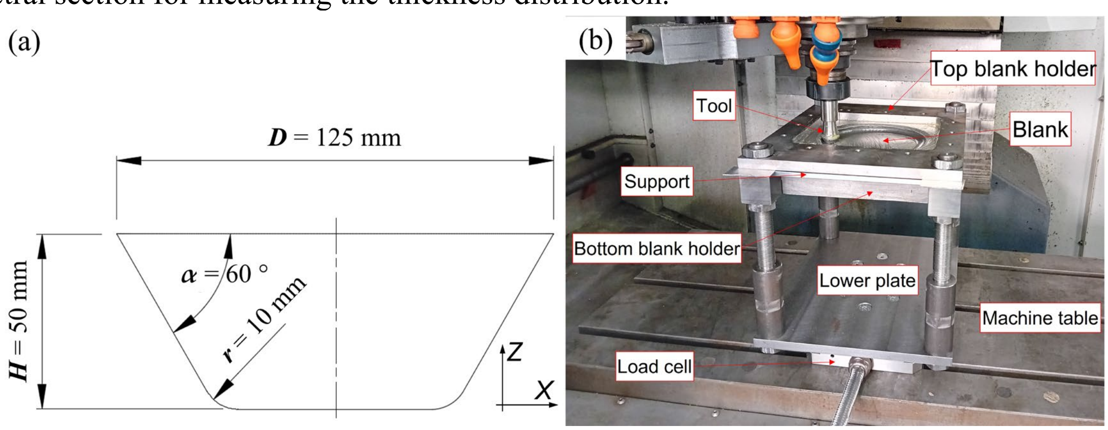

Fig. 2 (a) Frustum cone geometry and dimensions, and (b) SPIF equipment and setup.

Table 1 Chemical composition and mechanical properties of the blank material.

AA1050 H24 chemical composition						
Element % in weight	Al	Si	Cu	Fe	Mg	Mn
	99.50	<=0.25	<=0.05	<=0.40	<=0.05	<=0.05

For analyzing the effect of the proposed tool path strategies on the accuracy of the final part, FEM simulations of the SPIF process were developed by means of ABAQUS dynamic explicit software (Fig. 3). The support and the tool were modeled as analytically rigid surfaces. The former was fixed in the space, while the latter was moved accordingly to the related simulated strategy CN program. Shape and dimensions of them were defined in line to the experimental tests. The blank was modeled as a square shaped elasto-plastic deformable surface having a section thickness property of 1 mm. Each edge had a length of 150 mm and was fixed in the three spatial directions. It was discretized with a mesh consisting of squared shape shell elements. The dimension of these latter was varied in a range of 0.75-2.00 mm, at intervals of 0.25 mm, to perform a mesh convergency analysis. Its results revealed a forming load settlement at 1.25 mm; thus, this value was selected, leading to a total number of 14400 elements. The material flow stress σ was represented by the Hollomon power law [20] of Eq. 1, where ε, K, and n were the plastic strain, the strength coefficient, and the strain hardening exponent, respectively.

$$\sigma = K \cdot \varepsilon^n = 157 \cdot \varepsilon^{0.04} [MPa] \tag{1}$$

As reported in [15], since Hill's anisotropic yield criteria does not give significant FEM results improvement, Von Mises yield criteria was applied. The material elastic modulus and Poisson coefficient were set equal to 68 [GPa] and 0.33. Penalty method with a friction coefficient of 0.05 was set for modeling the blank-tool and the blank-support contact interfaces. A time step *dt* of 1×10^{-4} [s] was selected and mass scaling throughout the steps was applied to the whole model each 10 increments. Considering the lubrication condition and the low deformation heating generated during SPIF, FEM were performed in isothermal conditions.

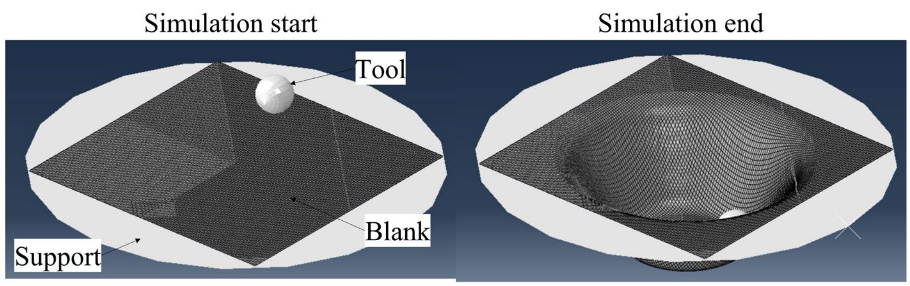

Fig. 3 FEM setup; start (on the left) and end (on the right) of the simulation for ModeS.

Fig. 4 shows the comparison of FEM and experimental (EXP) results for calibration (ModeS) and validation (ModeMD). The geometric comparison (Fig. 4a) was performed by importing the STL files of FEM and EXP achieved shapes in the GOM Inspect® software. After a best alignment phase, GOM depicts the deviations between geometries, permitting the point-to-point measurement of these latter and furnishing their distribution. The black line represents the experimental profile, while the colored one is referred to simulation. Negative or positive deviation labels' values correspond respectively to a geometry smaller or greater than the nominal one. The good superpositions of geometry, thickness distribution, and loads, are clearly visible, for both calibration and validation cases, enforcing FEM setup capability.

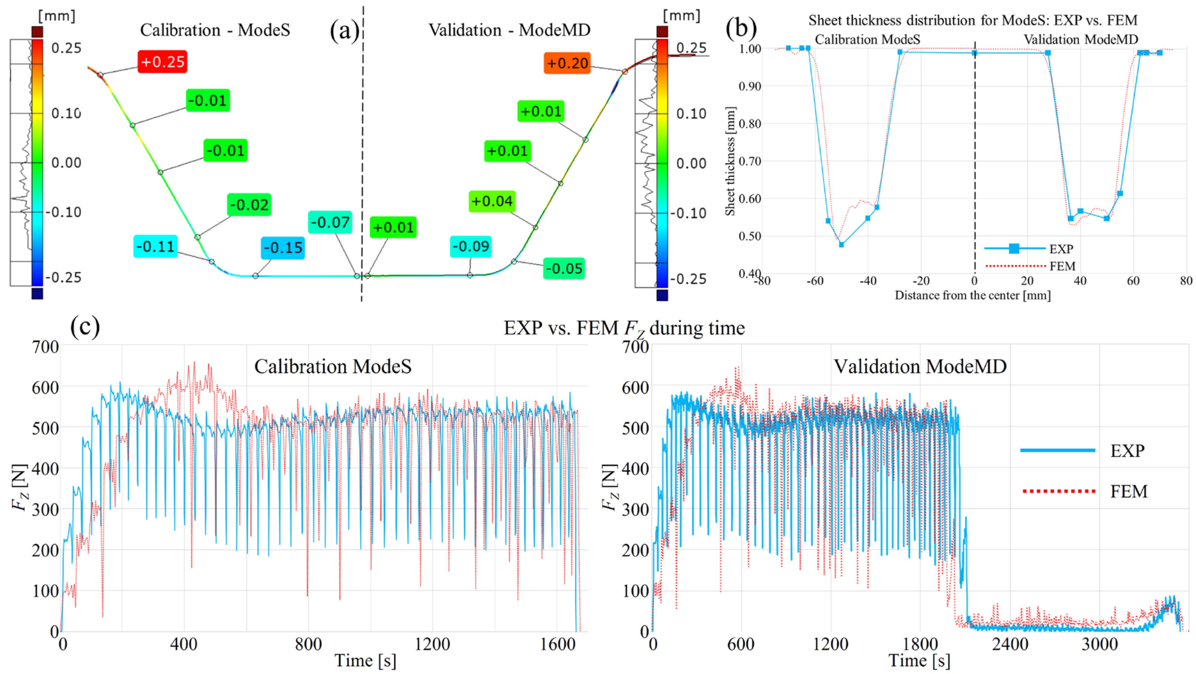

Fig. 4 EXP-FEM comparison of (a) geometry, (b) thickness and (c) force, for FEM validation

Results and discussion

All the strategies of Fig. 1 were simulated, exploiting the validated FEM setup, to individuate the one giving the best wall and bottom accuracy. The comparisons among FEM (black line) and nominal (colored) geometries, for the worst (ModeMA) and the best (ModeMD) strategy, are shown in Fig. 5. Table 2 summarizes the comparison results. $Wall_{Total}$ (Eq. 2) represents the maximum diametral deviation of the conical wall and is calculated by the summation of the correspondent two sides radial deviations ($Wall_1$ and $Wall_2$). *Pillow* is the bulge due to pillow effect, determined by Eq. 3 where, $Bottom_1$ and $Bottom_2$ are the deviations in the correspondence of the connecting radius amongst conical and bottom wall, while $Bottom_{Center}$ is the deviation on the revolution axis.

$$Wall_{Total} = Wall_1 + Wall_2 \tag{2}$$

$$Pillow = {Bottom_1 + Bottom_2}/_2 - Bottom_{Center} \tag{3}$$

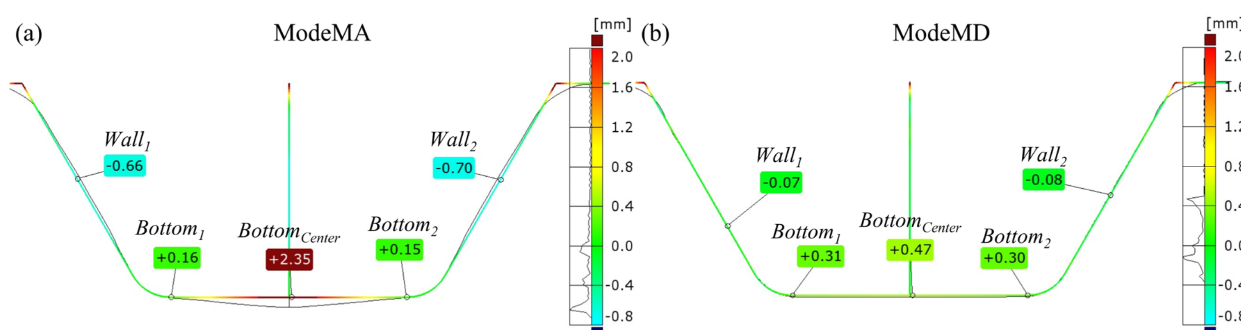

Fig. 5 GOM analysis of FEM resulting geometries for (a) the worst and (b) the best tool path strategy.

Table 2 Geometrical deviations of wall and bottom surface for the applied tool path strategies.

	Deviation value [mm]						
Mode	$Wall_1$	$Wall_2$	$Wall_{Total}$	$Bottom_1$	$Bottom_2$	$Bottom_{Center}$	*Pillow*
S	-0.57	-0.58	-1.15	+0.50	+0.47	+0.67	-0.19
MA	-0.66	-0.70	-1.36	+0.16	+0.15	+2.35	-2.19
MB	-0.65	-0.65	-1.30	+0.22	+0.23	+2.25	-2.02
MC	+0.08	+0.07	+0.15	+0.51	+0.52	+1.78	-1.26
MD	-0.07	-0.08	-0.15	+0.31	+0.30	+0.47	-0.16

Pillow results of ModeMA, ModeMB, and ModeMC shows that a direct contact of the tool in forming the bottom has an adverse effect on pillow accuracy. This is ascribable to the rigid body motion (Fig. 6) of the bottom material, as a consequence of the radial displacement of the tool after the axial penetration. In this case, the directions of the radial (F_r) and axial (F_z) forming force components are positioned outward and downward respectively. Therefore, the bottom is enlarged to the desired diameter but at excessive depth. Moreover, the rigid motion is increased by the material work-hardening at which it is subjected [12]. $Wall_{Total}$ values are lower for ModeMC and ModeMD highlighting the good influence of roughing-finishing approach. Even if the similar values of *Pillow* for ModeS and ModeMD are the lowest, the analysis of $Wall_{Total}$ suggests ModeMD as the most profitable strategy.

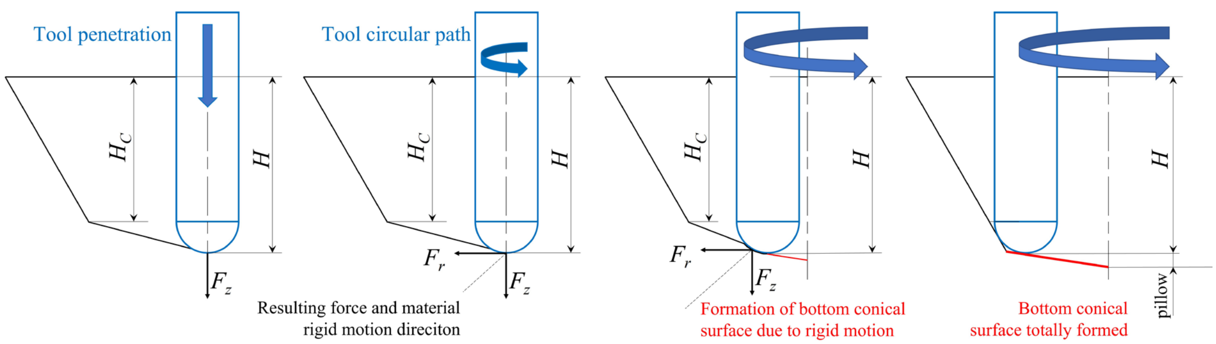

Fig. 6 Rigid motion of the material on the bottom part (red segment) due to the acting forces.

Fig. 7a graphs the z-components (F_Z) of the forming load for the totality of the analyzed strategies. In all the cases a force peak of 600 [N] is observable around a depth of 10 mm. During the remaining roughing phase, F_Z settles around 500 [N]. When working the bottom, after a first decreasing of F_Z, it reaches a second peak at 450 [N], while the axial finishing loads are lower than 100 [N] for all the strategies.

The sheet thickness distributions are represented in Fig. 7b, where the theoretical thickness t, calculated by the sine law of Eq. 4, in which α and t_i are the wall angle and the initial sheet thickness respectively, is reported as well.

$$t = t_i \cdot \sin\left({}^{\pi}/_{2} - \alpha\right) \tag{4}$$

Concerning Fig. 7b, directly working on the bottom results to be deleterious even on thickness distribution, with a reduction up to 0.9 mm in the central area; not detectable for ModeS and ModeMD. Conical walls show low thickness peaks in line with Eq. 4 but, a lower peak and a more uniform distribution is observable for ModeMD. As observed in [16], due to the low wall angle of roughing step, ModeMC presents the highest wall thickness, while, the lowest one is visible in the bottom region as a consequence of the material stretching in the F-B movement (Fig. 1e). Considering the better outcomes in terms of wall and bottom accuracy, homogeneity of thickness distribution, and forming loads, ModeMD results the most suitable strategy, even if a higher process time is requested.

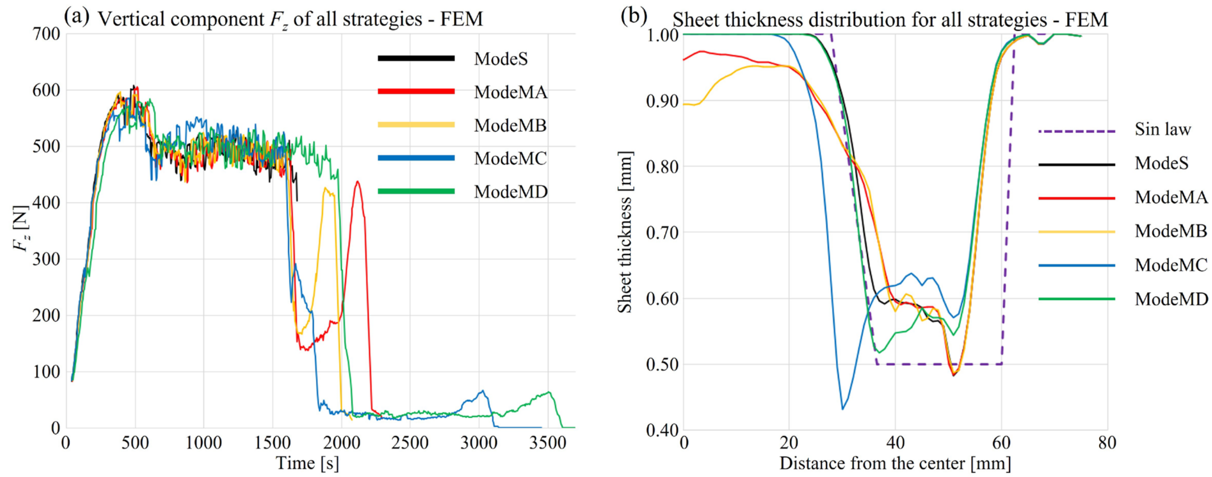

Fig. 7 Comparison of FEM resulting Fz (a) and thickness (b) for all the analyzed strategies.

Conclusions and future developments

In this paper, the influence of multi-step tool path strategies in SPIF manufacturing of AA1050-H24 frustum cones was analyzed by FEM simulations. In order to validate the simulation setup, the experimental results, in term of geometry, force and thickness, for a single-step methodology (ModeS), were compared with the numerical ones. Aimed to individuate the tool trajectory giving the best aforementioned results, four multi-step strategies, two concerning the complete forming of the cone bottom (ModeMA, ModeMB) and two consisting roughing-finishing passages (ModeMC, ModeMD), were then simulated. The FEM evidence pointed up the harmful influence on the pillow defect when, totally (ModeMA, ModeMB) or partially (ModeMC), forming the bottom, as a consequence of material rigid body motion. Moreover, a bottom reduction and an inhomogeneous distribution of thickness were detected. In contrast, a more uniform thickness and an enhanced accuracy resulted from the application of ModeMD, revealing it as the best strategy for the studied geometry. With the intention of reducing process times, additional works will be performed by increasing tool feed and varying process parameters. Likewise, supplementary investigations of the proposed strategies will be carried out on different materials.

References

[1] G. Mandaloi, A. Nagargoje, A.K. Gupta, G. Banerjee, H.Y. Shahare, P. Tandon, A Comprehensive Review on Experimental Conditions, Strategies, Performance, and Applications of Incremental Forming for Deformation Machining. Manuf. Sci. Eng. 144(11) (2022) 110802. https://doi.org/10.1115/1.4054683

[2] A.M. Rohit, C. Pandivelan, A critical review of incremental sheet forming in view of process parameters and process output, Adv. Mater. Process. Technol. 8(2) (2021) 2039-2068. https://doi.org/10.1080/2374068X.2021.1878730

[3] A. Gohil, B. Modi, Review of the effect of process parameters on performance measures in the incremental sheet forming process, Proc. Inst. Mech. Eng. B J. Eng. Manuf. 235(3) (2021) 303-332. https://doi.org/10.1177/0954405420961215

[4] S. Choudhary, A. Mulay, Influence of Tool Size and Step Depth on the Formability Behavior of AA1050, AA6061-T6, and AA7075-T6 by Single-Point Incremental Forming Process, J. Mater. Eng. Perform. 33 (2024) 3283-3298. https://doi.org/10.1007/s11665-023-08231-7

[5] S.M. Najm, I. Paniti, Study on Effecting Parameters of Flat and Hemispherical end Tools in SPIF of Aluminium Foils, Tehnički vjesnik, 27(6) (2020) 1844-1849. https://doi.org/10.17559/TV-20190513181910

[6] T. Trzepiecinski, S.M. Najm, V. Oleksik, D. Vasilca, I. Paniti, M. Szpunar, Recent Developments and Future Challenges in Incremental Sheet Forming of Aluminium and Aluminium Alloy Sheets, Metals 12 (2022) 124. https://doi.org/10.3390/met12010124

[7] H. Lu, H. Liu, C. Wang, Review on strategies for geometric accuracy improvement in incremental sheet forming, Int. J. Adv. Manuf. Technol. 102 (2019) 3381-3417. https://doi.org/10.1007/s00170-019-03348-3

[8] Z. Liu, Y. Li, P.A. Meehan, Tool path strategies and deformation analysis in multi-pass incremental sheet forming process, Int. J. Adv. Manuf. Technol. 75 (2014) 395-409. https://doi.org/10.1007/s00170-014-6143-6

[9] M. Skjoedt, M.B. Silva, P.A.F. Martins, N. Bay, Strategies and limits in multi-stage single-point incremental forming, J. Strain Anal. Eng. Des. 45(1) (2010) 33-44. https://doi.org/10.1243/03093247JSA574

[10] D. Xu, R. Malhotra, N.V. Reddy, J. Chen, J. Cao, Analytical prediction of stepped feature generation in multi-pass single point incremental forming, J. Manuf. Proc. 14 (2012) 487-494. https://doi.org/10.1016/j.jmapro.2012.08.003

[11] Z. Liu, Y. Li, P.A. Meehan, Vertical Wall Formation and Material Flow Control for Incremental Sheet Forming by Revisiting Multistage Deformation Path Strategies, Mater. Manuf. Proc. 28(5) (2013) 562-571. https://doi.org/10.1080/10426914.2013.763964

[12] G. Buffa, M. Gucciardi, L. Fratini, F. Micari, Multi-directional vs. mono-directional multi-step strategies for single point incremental forming of non-axisymmetric components, J. Manuf. Process. 55 (2020) 22-30. https://doi.org/10.1016/j.jmapro.2020.03.055

[13] S. Wu, L. Gao, Y. Matsuoka, S. Rashed, Y. Zhao, N. Ma, Multi-step toolpath approach of improving the dimensional accuracy of a nonaxisymmetric part in incremental sheet forming and its mechanism analysis, J. Mech. Sci. Technol. 36(4) (2022) 1975-1985. https://doi.org/10.1007/s12206-022-0333-1

[14] C. Henrard, C. Bouffioux, P. Eyckens, H. Sol, J.R. Duflou, P. Van Houtte, A. Van Bael, L. Duchene, A.M. Habraken, Forming forces in single point incremental forming: prediction by finite element simulations, validation and sensitivity, Comp. Mech. 47 (2011) 573-590. https://doi.org/10.1007/s00466-010-0563-4

[15] P. Eyckens, J.R. Duflou, A. Van Bael, P. Van Houtte, The significance of friction in the single point incremental forming process, Int. J. Mater. Form. 3(1) (2010) 947-950. https://doi.org/10.1007/s12289-010-0925-7

[16] S. Wu, Y. Ma, L. Gao, Y. Zhao, S. Rasheda, N. Ma, A novel multi-step strategy of single point incremental forming for high wall angle shape, J. Manuf. Proc. 56 (2020) 697-706. https://doi.org/10.1016/j.jmapro.2020.05.009

[17] Z. Chang, M. Yang, J. Chen, Geometric deviation during incremental sheet forming process: Analytical modelling and experiment, Int. J. Mach. Tools Manuf. 198 (2024) 104160. https://doi.org/10.1016/j.ijmachtools.2024.104160

[18] M. Murugesan, H.W. Youn, J.H. Yu, W. Chung, C.W. Lee, Investigation of forming parameters influence on pillow defect in a new vacuum-assisted incremental sheet forming

process, Int. J. Adv. Manuf. Technol. 127 (2023) 5531-5551. https://doi.org/10.1007/s00170-023-11854-8

[19] B.B.L. Isidore, G. Hussain, S.P. Shamchi, W.A. Khan, Prediction and control of pillow defect in single point incremental forming using numerical simulations, J. Mech. Sci. Technol. 30 (2016) 2151-2161. https://doi.org/10.1007/s12206-016-0422-0

[20] R. Perez-Santiago, N.J. Hendrichs, G. Capilla-González, E. Vázquez-Lepe, E. Cuan-Urquizo, The Influence of the Strain-Hardening Model in the Axial Force Prediction of Single Point Incremental Forming, Appl. Sci. 14 (2024) 5705. https://doi.org/10.3390/app14135705